Isothermal Solid-State Transformation Kinetics Applied to Pd/Cu Alloy Membrane Fabrication

Natalie Pomerantz and Yi Hua Ma
Center for Inorganic Membrane Studies, Dept. of Chemical Engineering, Worcester Polytechnic Institute, Worcester, MA 01609

E. Andrew Payzant
Materials Science and Technology Div., Oak Ridge National Laboratory (ORNL), Oak Ridge, TN 37831

DOI 10.1002/aic.12217
Published online March 22, 2010 in Wiley Online Library (wileyonlinelibrary.com).

In this work, time-resolved, in situ high-temperature X-ray diffraction was used to study the solid-state transformation kinetics of the formation of the fcc Pd/Cu alloy from Pd/Cu bilayers for the purpose of fabricating sulfur-tolerant Pd/Cu membranes for H_2 separation. Thin layers of Pd and Cu (total ~15 wt % Cu) were deposited on porous stainless steel with the electroless deposition method and annealed in H_2 at 500, 550, and 600°C. The kinetics of the annealing process was successfully described by the Avrami nucleation and growth model, showing that the annealing process was diffusion controlled and one dimensional. The activation energy for the solid-state transformation was 175 kJ/mol, which was similar to the activation energy of Pd-Cu bulk interdiffusion. Furthermore, the Avrami model was able to successfully describe the changes in permeance and activation energy observed in Pd/Cu alloy membranes during characterization as they were annealed at high temperatures. © 2010 American Institute of Chemical Engineers *AIChE J*, 56: 3062–3073, 2010

Keywords: Pd membranes, Pd/Cu alloys, Pd/Cu diffusion, time-resolved, in situ high-temperature X-ray diffraction, Avrami model

Introduction

Hydrogen-selective Pd membranes can improve the efficiency and cost effectiveness of the coal gasification process by recovering high-purity H_2 from the syngas. Cap and trade agreements and legislation have been implemented to require industrial plants to limit their CO_2 emissions if not ceasing them entirely. The retentate stream from the hydrogen-permeable membrane reactor in a coal gasification process would already consist of high-pressure CO_2, thus reducing the energy needed for the pressurization stage of carbon capture required for carbon sequestration.[1]

Thin film Pd and Pd alloy membranes supported on porous metal substrates have both strength and structural integrity stemming from the support. Similar coefficients of thermal expansion between the Pd layer and the metal support ensure thermal stability over a wide range of temperatures. In addition, the tubular metal supports allow for a simple membrane reactor design, making the composite Pd membranes well suited for industrial applications. Of the various methods for depositing Pd films, electroless deposition in particular meets industrial needs because the thin, hard film covers all surfaces of the support evenly with good adhesion, and the process is easy to scale up, ensuring a high H_2 permeance and low cost.

However, only a few ppm of H_2S present in the gas stream will poison and reduce the H_2 permeance of the Pd membrane, in some cases causing irreparable damage.[2–5] Pd/Cu alloys have generated much research, because of their resistance to H_2S poisoning. It is well known that the enhanced H_2S resistance only occurs when the membrane is

Correspondence concerning this article should be addressed to Yi Hua Ma at yhma@wpi.edu.

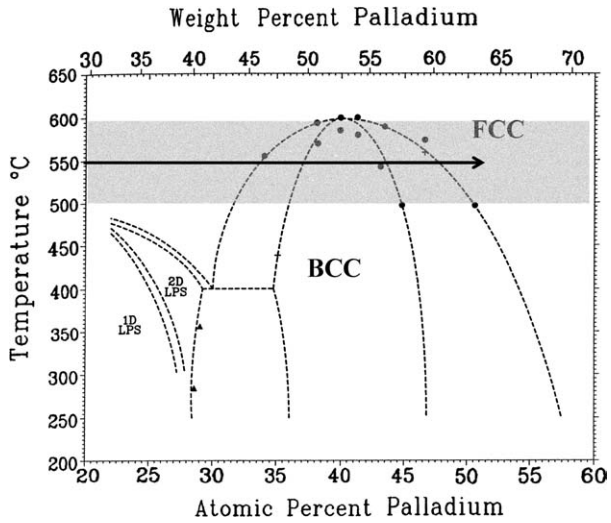

Figure 1. Pd-Cu phase diagram.[6]

The gray area indicates the temperature range tested in this work.

in the fcc region of the Pd/Cu phase diagram (see Figure 1[6]),[2,3,5,7] the disadvantage being that the fcc Pd/Cu membranes have a lower permeance than Pd and other Pd alloy membranes.[8–10] As H_2S poisoning occurs near the surface, an fcc alloy on the top layer of the Pd membrane protects the surface of the membrane without greatly reducing the permeance.[11]

As there is no Pd-Cu codeposition bath known in the literature, preparation of the Pd/Cu alloy membrane from the electroless deposition method requires the plating of sequential layers of Pd and Cu resulting in a bilayer followed by the annealing of that bilayer. Although there has been research in the past, which briefly investigated the formation of the bcc alloy from Pd/Cu bilayers with ex situ methods,[12] and work, which studied the kinetics of the fcc-bcc Pd/Cu phase transformation in a thin homogenous Pd/Cu layer,[13] there has been no in-depth in situ investigation into the formation of the sulfur-tolerant fcc Pd/Cu alloy from Pd/Cu bilayers.

In the past, high-temperature X-ray diffraction (HT-XRD) has been used to monitor the phase transformations in situ, which occurred as a result of a product film forming from a thin film of bilayers. The time-resolved measurements enabled kinetic constants to be obtained from the formation of $CuGaSe_2$ from GaSe/CuSe bilayers[14] and $CuInSe_2$ from InSe/CuSe bilayers[15] and provided a greater understanding of the mechanism of the phase transformations. Of particular relevance to this work is the HT-XRD investigation of the Pd/Ag alloy formation from Pd/Ag bilayers,[16] which, through an investigation of the phase transformation, attained both qualitative and quantitative information with regards to Pd/Ag alloy membrane fabrication and permeance characteristics.

The main objective of this work was to use the time-resolved, in situ HT-XRD to investigate the annealing conditions required to form an fcc alloy from a deposited Pd/Cu bilayer, to understand the mechanism of the annealing process with the purpose of applying that knowledge to the fabrication of sulfur-tolerant Pd/Cu membranes, and to understand the change in permeation at higher temperatures as a result of phase change.

Experimental

Sample preparation

The metal substrates used in this study were provided by Mott Metallurgical. Sheets of 316L porous stainless steel (PSS) with a 0.5-μm media grade were cut into coupons (dimensions: 1 cm $\times$ 1 cm $\times$ 0.1 cm). Porous supports used for membrane permeation experiments were Inconel tubes (dimensions: length, 6 cm; OD, 1.25 cm; thickness, 0.16 cm) and welded to nonporous 316L SS at both ends with a cap on one end. All porous metals were cleaned to remove dirt and grease with an alkaline solution including 5 ml/l of a saturated solution of industrial detergent. The PSS coupons and Inconel supports were oxidized at 800 and 700°C, respectively, for 12 h to form an oxide intermetallic diffusion barrier[17] between the support metals and the Pd alloy layer.

The supports were sensitized and activated with Pd nuclei according to the procedure outlined previously.[18] Before plating, the activated supports were dipped in 1 M HCl for 30 s and then in DI (deionized) water. The plating bath compositions are listed in Table 1, and the plating procedure was detailed by Mardilovich et al.[18] The Cu plating bath, shown in Table 1, was adapted from Ma et al.[19] After the electroless deposition of Cu, the samples were immediately immersed in 0.01 M HCl to neutralize any residual plating solution followed by rinsing with DI water and ethanol to facilitate drying to prevent oxidation of the Cu layer. The resultant layer thicknesses and compositions are listed in Table 2.

The average thicknesses of the deposited metals were determined gravimetrically: the weight gain of the sample divided by the product of the plated surface area and the metal density. The membranes were plated until dense, as described previously.[18]

With regards to applying the coupon study to membrane fabrication, the thickness of the Pd alloy layers (10–20 μm) deposited on both the flat coupons and the tubular supports was smaller than the radius of the tube (0.625 cm) by over two orders of magnitude. Therefore, it was expected that the effect of the curvature of the tubular support could be neglected and a one-dimensional flat plate geometry applied in both cases.

Table 1. Plating Bath Compositions and Conditions

	Pd Bath	Cu Bath
$Pd(NH_3)_4Cl_2 \cdot H_2O$ (g/l)	4	
$CuSO_4 \cdot 5H_2O$ (g/l)		25
$Na_2EDTA \cdot 2H_2O$ (g/l)	40.1	47.5
NH_4OH (28%) (ml/l)	198	
H_2NNH_2 (98%) (ml/l)	0.19	
H_2CO (37%) (ml/l)		25
EDA (ppm)		112
$K_4Fe(CN)_6 \cdot 3H_2O$ (ppm)		35
$(C_2H_5)_2NCS_2Na \cdot 3H_2O$ (ppm)		5
pH	10–11	12.0
Temperature (°C)	60	20–25

Table 2. Samples Tested in this Work

Annealing Temperature (°C)	Substrate	Pd Layer (μm)	Cu Layer (μm)	Cu (wt %)
As-deposited	PSS	13.1	4.1	19
500	PSS	13.0	2.6	13
550	PSS	13.4	3.5	16
600	PSS	12.8	3.2	15

Surface and cross-sectional analysis

Surface and cross-sectional characterizations were carried out with the Amray 1610 Turbo scanning electron microscope (SEM) equipped with a Princeton Gamma-Tech Avalon energy-dispersive X-ray (EDX) light element detector and a RBA-1610 5MC type Robinson retractable backscattered electron detector for qualitative and quantitative elemental analysis. The spatial resolution for SEM-EDX lay between 0.8 and 1.2 μm, and the penetration depth was about 1 μm for the samples investigated. To obtain cross sections, the samples were cut with a SiC saw blade and mounted in phenolic powder with a Smithells II mounting press. The samples were ground with SiC paper of increasing fineness from 60 to 2400 grit with the Metaserv 2000 grinder polisher. The samples were further polished with α-Al_2O_3 slurries consisting of particles of increasing fineness from 1, 0.3 to 0.05 μm. Before the cross-sectional analysis, samples were sputter coated using a gold/palladium target to avoid charging.

X-ray diffraction procedures

The time-resolved, in situ HT-XRD experiments were performed at Oak Ridge National Laboratories. The diffraction data were collected with the PANalytical X'Pert Pro θ/θ MPD/X-ray diffractometer (Cu Kα radiation source operated at 45 kV and 40 mA) equipped with an Anton Paar XRK-900 furnace, which allowed the temperature to be varied between 25 and 900°C. A Macor sample holder supported the sample in the furnace. The electrical heater of the furnace was designed to heat the volume of the sample with a minimal temperature gradient. A PANalytical X'celerator real-time multiple-strip detector was used to rapidly collect the data. A vacuum was applied while heating the samples to 250°C at a rate of 50°C/min. At 250°C, a pure H_2 atmosphere was introduced at a pressure of 1 bar, and the temperature was increased to the final annealing temperature at a rate of 50°C/min. The scans ranged from 2Θ values of 37°–45°, and the total time of the scan varied from 30 s to 30 min, depending on the rate of phase change.

The quantitative analysis of the diffraction data was carried out with the software X'Pert Highscore Plus using a Le-Bail fit and a flat background. The weight fractions were calculated by the direct comparison method of the integrated peak intensities.[20] At high temperatures, there was a significant overlap between the bcc (1 1 0) and Cu (1 1 1) peaks. A standard of Cu plated on oxidized PSS was heated to each of the temperatures tested in this work and scanned to determine the peak position.

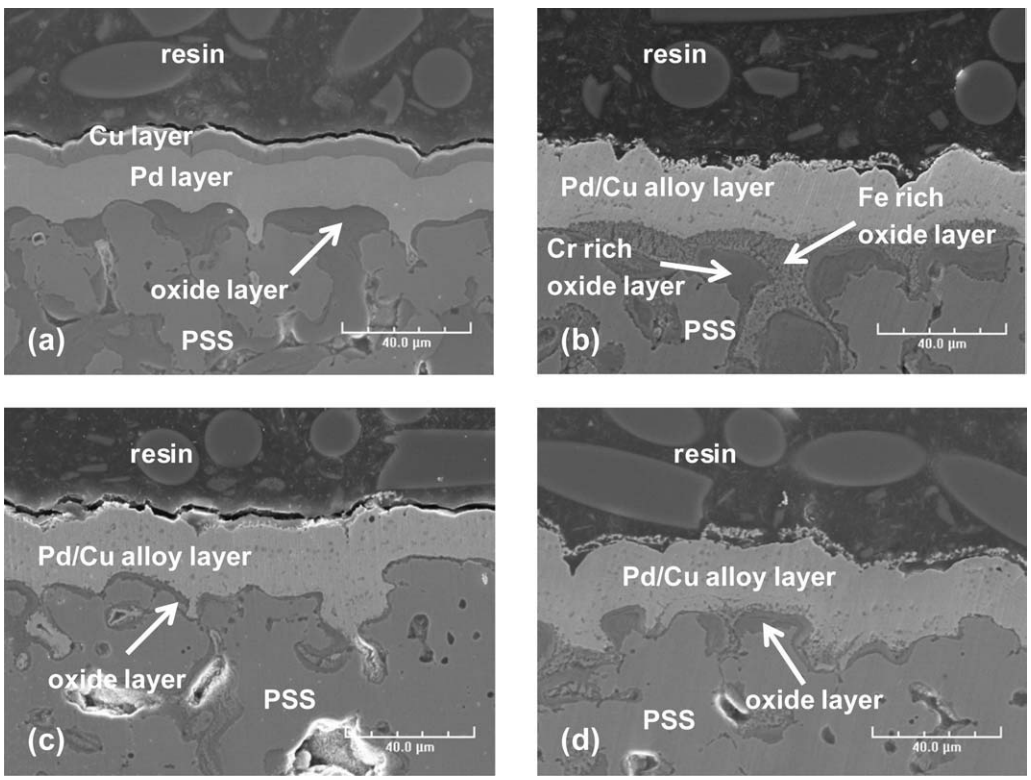

Figure 2. Cross-sectional micrographs at ×1000 for the PSS samples.

(a) As-deposited, and annealed at (b) 500°C, (c) 550°C, and (d) 600°C.

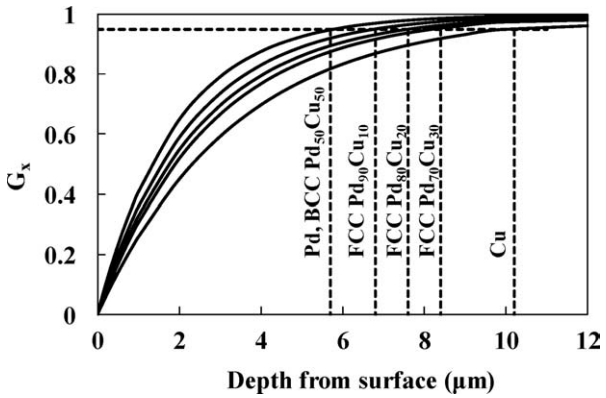

Figure 3. Fraction of the diffracted intensity (G_x), which was contributed by a surface layer of depth x for Pd, Cu, and Pd/Cu alloys from the (1 1 1) plane of the fcc lattice structure and the (1 1 0) plane of the bcc lattice structure.

The penetration depth is shown with dotted lines, taken from $G_x = 0.95$.

Membrane permeation testing

The membranes were tested in a shell and tube apparatus encased in a furnace. The tube side was equipped with a sweep and the feed line connected to a ballast volume to ease the transition when changing between H_2 and He gases. The experimental set up and testing procedures were described in detail previously.[11]

Results

Cross-sectional analysis

Figure 2a shows the cross section of an as-deposited Cu/Pd/PSS sample. The oxide intermetallic diffusion barrier layer appeared relatively uniform on the PSS. The Pd layer covered the surface of the substrate and entered some of the pores. The average thickness of the Pd layer was 10 μm, and the average thickness of the Cu layer was 4.7 μm, which was close to the gravimetric estimate of Cu shown in Table 2. The Pd layer thickness was less than the gravimetric estimate shown in Table 2 because of the penetration of Pd inside the pores, which was not included in the visual approximation of the thickness from the micrograph.

It should be noted that the penetration depth of the XRD did not encompass the entire depth of the Pd/Cu bilayer, and the phases detected were limited to those present in the penetration depth, which ranged from 5.5 to 8.5 μm depending on the Cu concentration of the fcc or bcc alloy, shown in Figure 3. The penetration depth was calculated according to Eq. 1, where G_x is the diffracted intensity at a distance, x, from the surface and μ is the linear absorption coefficient.[20]

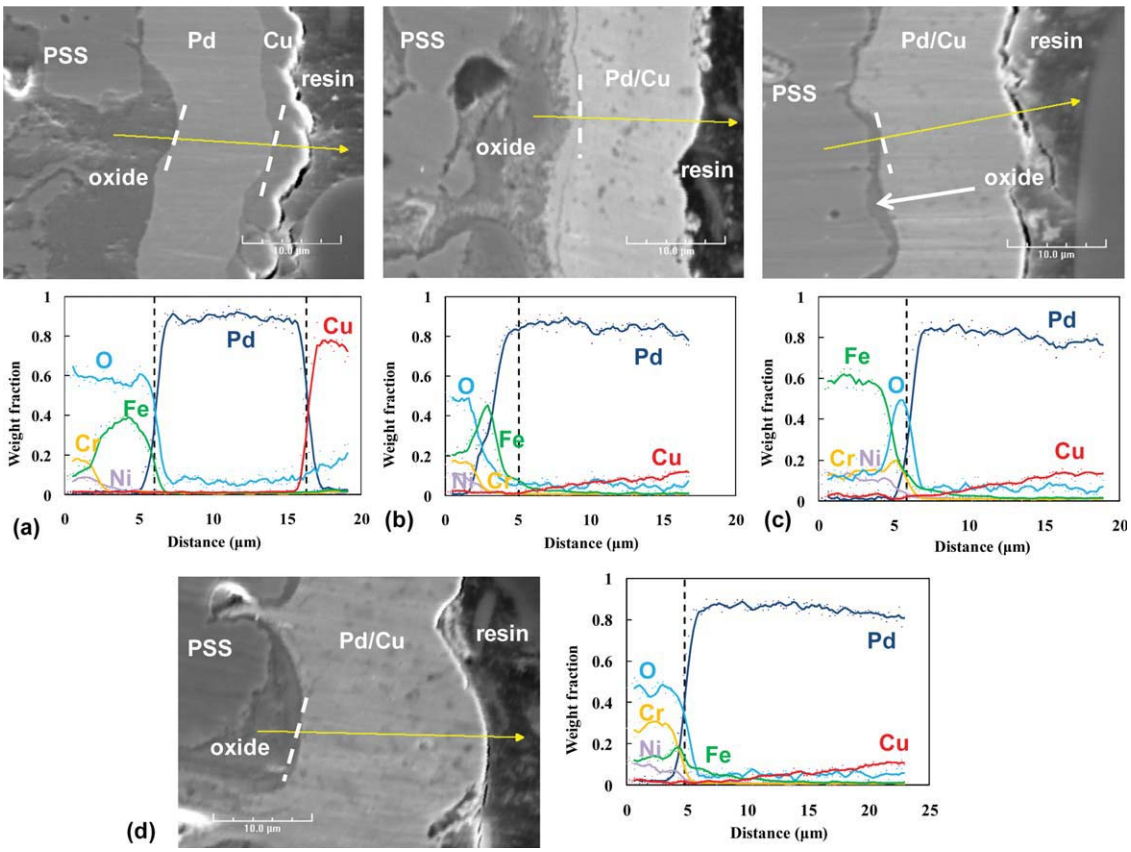

Figure 4. Cross-sectional micrographs at ×3000 and corresponding elemental line scans for the samples.

(a) As-deposited, and annealed at (b) 500°C, (c) 550°C, and (d) 600°C. [Color figure can be viewed in the online issue, which is available at wileyonlinelibrary.com.]

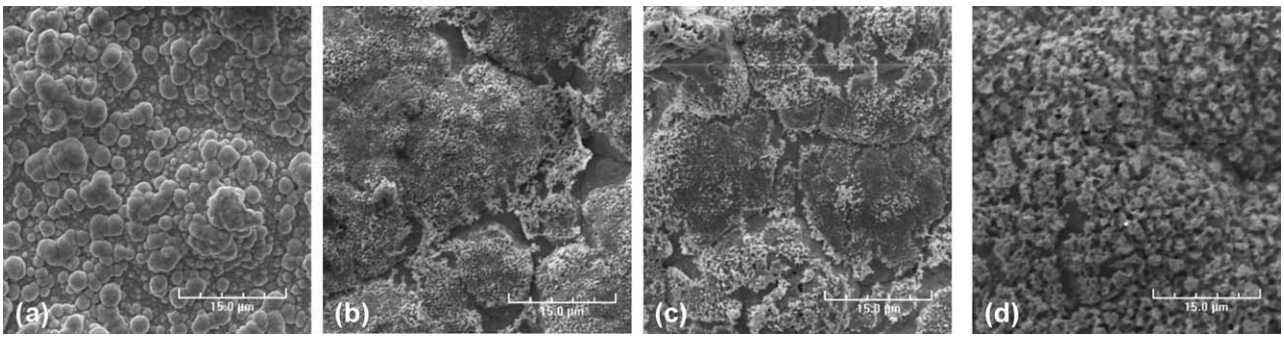

Figure 5. Surface micrographs at ×2000 for the samples.

(a) As-deposited, and annealed at (b) 500°C, (c) 550°C, and (d) 600°C.

$$G_x = 1 - \exp\left\{-\frac{2\mu x}{\sin\theta}\right\}. \quad (1)$$

Figures 2b–d show the cross sections of the Pd/Cu/PSS samples annealed in H_2 at 500, 550, and 600°C for 50, 25, and 8 h, respectively. In all three Pd/Cu layers, the contrast between the Pd and Cu layers disappeared after the Pd/Cu alloy formed. In addition, a porous Pd/Cu alloy, which was approximately half the thickness of the original Cu deposit, had formed on top of a nonporous Pd/Cu alloy. The porous Pd/Cu alloy detached from the nonporous Pd/Cu alloy surface during the mounting and grinding process as described in the Experimental section. The porous Pd/Cu alloy is described further in the analysis of the surface morphology.

Figure 4a shows the cross section and corresponding elemental line scan at ×3000 of the as-deposited Cu/Pd/PSS sample. The boundary between the Cu and Pd layers was clearly seen at a distance of 16 μm. The increase in the oxygen content seen after 16 μm was most likely caused by the slight surface oxidation of the cross-sectional surface of the pure Cu. Annealing Cu with Pd prevented copper oxides forming at room temperature, and the surface of the cross section of the Pd/Cu layers in Figures 4b–d did not see an increase in oxygen content. The oxide layer of the support in Figure 4a was rich in Fe toward the surface of the Pd layer possibly because of the enhancement of the Fe diffusion at higher oxidation temperatures.[21] The Cr_2O_3, which was more stable in H_2 atmospheres,[21] was more prevalent farther away from the Pd layer, also seen previously.[18] In Figure 4b, the decrease in oxygen with the oxide toward the interface of the Pd/Cu layer was accompanied by a decrease in Cr, showing that although part of the iron oxide was reduced during the annealing in H_2, the chromium oxide remained. The two distinct oxides are seen very clearly in Figure 2b, as determined by EDX.

Figures 4b–d show that the high-temperature annealing in H_2 caused the Cu to diffuse to form fcc Pd/Cu alloys with a varying Cu content. The largest amount of Cu was found on the surface of the Pd/Cu layer. After eliminating the contributions of the support metals and oxygen to the line scans in Figure 4, the total weight percent of Cu on the surface of the Pd/Cu layers was 16, 17, and 12 wt % for the samples annealed at 500, 550, and 600°C, respectively. Several line scans were taken of each sample at various locations including where the Pd/Cu layer filled the pores of the PSS and where the layer covered the top surface of the PSS. The range of the Cu content seen near the surface varied from 8 to 15, 12 to 18, and 10 to 16 wt % for the samples annealed at 500, 550, and 600°C, respectively. The Cu gradient and range of the Cu content at the interface between the mounting resin and the surface of the Pd/Cu layer were similar for all of the samples, independent of temperature.

According to the Pd-Cu phase diagram in Figure 1, the miscibility gap for the fcc–bcc phase transition begins at 45 wt % Cu at 600°C, 40 wt % Cu at 550°C, and 38 wt % Cu at 500°C. The gap widens with decreasing temperature; however, for the temperatures tested, the Cu concentrations of the annealed Pd/Cu layers as measured by EDX would correspond to the fcc region of the phase diagram.

Surface morphology

Figure 5a shows the surface morphology of the Pd/Cu bilayer before the annealing. Some of the Cu clusters of the deposit appeared to be larger than others; however, EDX analysis showed that the Cu covered the entirety of the Pd layer, and the cross-sectional micrograph in Figure 4a confirmed that the layer was uniform in thickness. After annealing, the morphology changed to a porous Pd/Cu alloy over a nonporous Pd/Cu alloy (see Figures 5b–d). The porous Pd/Cu alloy was caused by the Kirkendall effect,[22] which occurred when two metals underwent interdiffusion and the diffusion coefficients were unequal. In this case, the voids formed when Cu atoms diffused faster than the Pd atoms. Kirkendall porosity has been observed previously on the Cu side of Pd/Cu diffusion couples.[23]

Another reason for the voids could be from the fcc–bcc transition. Indeed, the change in the lattice structure and the lattice parameter could cause irreversible structural changes. Yuan et al.[24] observed H_2 permeation hysteresis in Pd/Cu membranes after temperature cycling to induce the fcc–bcc phase transformation. However, the hysteresis was attributed to a metastable hydrogenated PdCu(H) fcc phase.

Elemental analysis performed with EDX showed that the Cu concentration varied between 5 and 20 wt % on the surfaces of the annealed samples, indicating a concentration within the fcc region of the phase diagram.[6] As with the cross-sectional analysis, the surface concentration had a similar range independent of temperature.

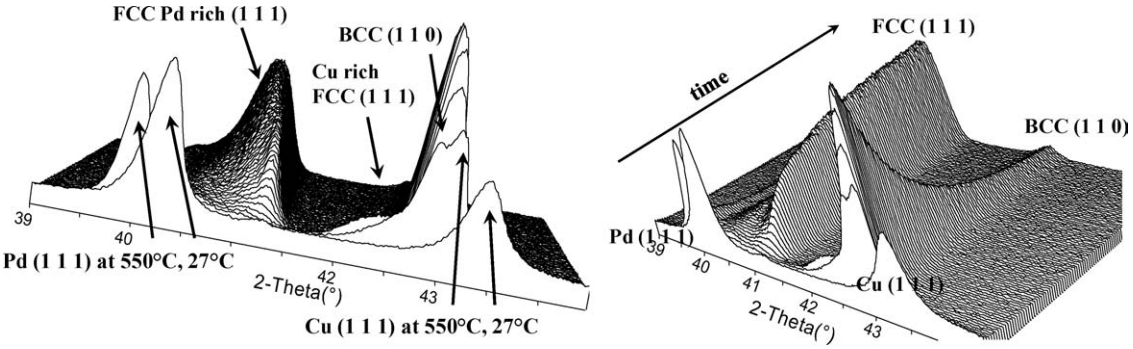

Figure 6. XRD scans as a function of time at 550°C.

Time-resolved, in situ HT-XRD

During the annealing process, between the temperatures of 500 and 600°C, there can be a maximum of five phases present: the pure Pd and pure Cu phases, the Pd-rich and Cu-rich fcc phases, and the bcc phase, seen in Figure 1. Figure 6 shows the X-ray diffraction data as time progressed for the coupon annealed at 550°C in H_2. Before the annealing process began, the only phases present were from the bilayers of Cu and Pd. The diffusion of Cu brought on by heating caused five phases to form with the phases the most rich in Cu toward the surface of the sample.

The first pattern in Figure 6 shows the peaks of the (1 1 1) plane for both Pd and Cu at room temperature. The second pattern was taken at 550°C and showed the peak shift of both the Pd (1 1 1) and Cu (1 1 1) planes to a lower value of 2Θ because of the thermal expansion of the lattice. Also, the peak representing the (1 1 0) plane of the bcc phase of the Pd/Cu alloy appeared next to the Cu (1 1 1) peak, with significant overlap. The left tail of the bcc (1 1 0) peak showed the Cu-rich fcc phase (1 1 1) peak forming. The width of the peak attested to the concentration gradient within the Cu-rich fcc phase. As time progressed, the Cu (1 1 1) and Cu-rich fcc (1 1 1) peaks disappeared, the Pd (1 1 1) and bcc (1 1 0) peaks became smaller, and the Pd-rich fcc (1 1 1) peak increased in size.

As Cu diffused into the Pd layer, the Cu-rich phases and pure Pd phase disappeared with only the Pd-rich fcc and bcc phases remaining. Further interdiffusion caused the interface between the bcc and Pd-rich fcc phases to move toward the surface of the Cu deposit. If enough time was to pass, the bcc phase would eventually disappear leaving the Pd/Cu layer a homogeneous alloy entirely in the Pd-rich fcc phase with a Cu concentration of 16 wt % (from Table 2).

Figure 7 shows the weight fraction for all of the phases as a function of time for the sample annealed at 500°C. The pure Cu phase decreased sharply at the onset of the annealing, while the pure Pd phase gradually decreased. Contrary to the continuously decreasing Cu and Pd or the continuously increasing Pd-rich fcc phase, the Cu-rich fcc and the bcc phases both had maxima. The Cu-rich fcc phase increased until 30 wt % at 50 min after which the wt % decreased until it could barely be detected. Similarly, the bcc phase increased until a maximum was reached at 61 wt % at ~1000 min. The maxima appeared because the Cu-rich fcc and bcc phases were interim alloy phases, which formed before the Pd-rich fcc phase. The arrow in Figure 1 describes the annealing process of the bilayer surface.

The diffusion and consequently the rate of phase transformation significantly slowed down with time. In Figure 7, the pure Pd composition decreased from 11 to 5 wt % within the first 400 min and then decreased another 0.5 wt % over the next 2500 min. In Figure 8, the sample annealed at 550°C showed that the pure Pd phase was undetectable after 1000 min, and in Figure 9, the sample annealed at 600°C showed that the pure Pd phase was undetectable after only 400 min.

The decrease in the rate of the phase change was due in part to a lessening of the driving force as the concentration gradient of Cu in the sample became less steep and also due to the decreasing of the average diffusion coefficient as the sample alloyed. The Cu-Pd interdiffusion coefficient varied by two orders of magnitude depending on the alloy composition.[25] The value was highest at Cu compositions of roughly 70 wt % and lowest at 0 wt %. Cu had a lower Tamman temperature than Pd (405 and 640°C, respectively) and therefore became mobile due to thermal vibrations at a lower temperature than Pd. The result was that Cu diffused into the Pd very quickly but as more Cu diffused into the Pd, more Pd would have to diffuse into the Cu from deeper within the bilayer where the interdiffusion coefficient would be smaller and the driving force much less.

The pure Pd phase present within the penetration depth of the Pd/Cu layer (5.5–8.5 μm, see Figure 3) annealed at 550 and 600°C disappeared, while the amount of pure Pd phase

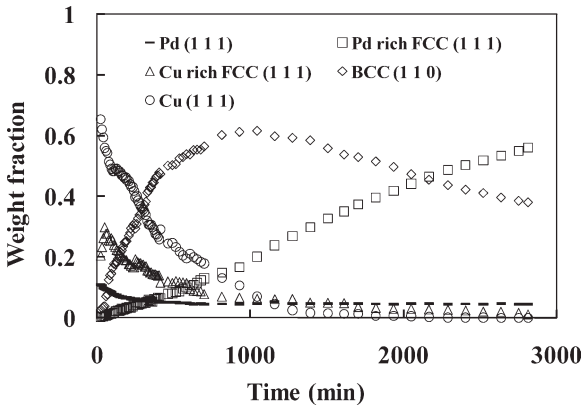

Figure 7. Weight fraction of the Pd-Cu phases as a function of time during annealing in H_2 at 500°C.

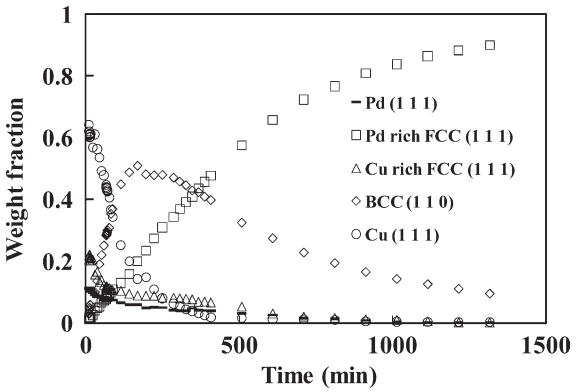

Figure 8. Weight fraction of the Pd-Cu phases as a function of time during annealing in H_2 at 550°C.

present in the coupon annealed at 500°C decreased very slowly after 400 min so that the amount appeared to not change at all. As the Cu diffused farther into the Pd layer, more heat and time were necessary for the transformation to progress. At 550 and 600°C, there was enough thermal energy to increase the diffusivity to cause the Pd phase to disappear from the XRD penetration depth.

The slowing down of the diffusion process and consequently the phase transformation between the Pd-rich fcc phase and the bcc phase is shown in Figures 7–9. At higher temperatures, less of the bcc phase and more of the Pd-rich fcc phase were present toward the end of the annealing. In addition, the maxima of the progression of the bcc phase weight fraction with time decreased with increasing temperature. The maxima were 61, 51, and 30 wt % at 500, 550, and 600°C, respectively. The decrease was due to the shape of the phase diagram, shown in Figure 1. The miscibility gap where the bcc phase formed decreased in width with increasing temperature, resulting in less of the bcc phase forming at higher temperatures.

Kinetic analysis

A kinetic study of the phase growth was used to obtain qualitative information about the mechanism of the annealing process as well as quantitative information by estimating the rate constants. The Avrami model[26–28] states that the new phase first appears in the form of nuclei dispersed throughout the previous phase. The nuclei grow three dimensionally into spherical grains. As the grains grow, they impinge upon each other, consequently slowing down the growth process as the transformation completes. The model is expressed in Eq. 2, where f is the fraction of the new phase, n is the Avrami exponent, which is dependent on the reaction mechanism, nucleation rate, and nuclei geometry, and k is the kinetic rate constant, which is dependent on temperature, the size of the nuclei, the number of nucleation sites, and the nuclei growth rate.

$$f = 1 - \exp\{-(kt)^n\}. \tag{2}$$

The rate constants were calculated through the linearization of Eq. 2, shown in Eq. 3:

$$\ln[-\ln(1-f)] = n\ln k + n\ln t. \tag{3}$$

Figure 10 shows the linear regression of Eq. 3 for the Cu/Pd/PSS samples annealed between 500 and 600°C. The exponents for the Avrami model are listed in Table 3 and are all ~1.1. Hulbert[29] has advocated the Avrami model in the past and shown mathematically that Avrami exponents between the values of 0.5 and 1.5 indicated a diffusion-controlled, one-dimensional growth process with a decreasing nucleation rate, and the exponents between the values of 1 and 2 indicated a phase-boundary controlled, one-dimensional growth process with a decreasing nucleation rate. Avrami exponents equaling 1 indicated one-dimensional growth, which was phase-boundary controlled with a zero nucleation rate or saturation of the point sites. The one-dimensional growth was explained as the thickening of needles or rods, which had undergone complete edge impingement; in this case, forming the layer of the new phase as it thickened.[30]

Previous studies involving product layers forming from bilayers of Pd/Ag,[16] GaSe/CuSe,[14] and InSe/CuSe[15] have resulted in low Avrami exponents ($0.3 < n < 0.8$) showing

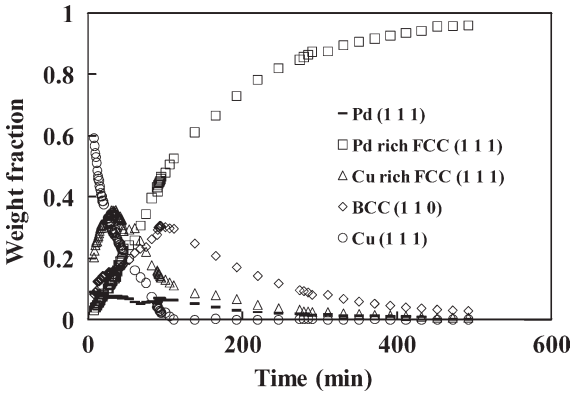

Figure 9. Weight fraction of the Pd-Cu phases as a function of time during annealing in H_2 at 600°C.

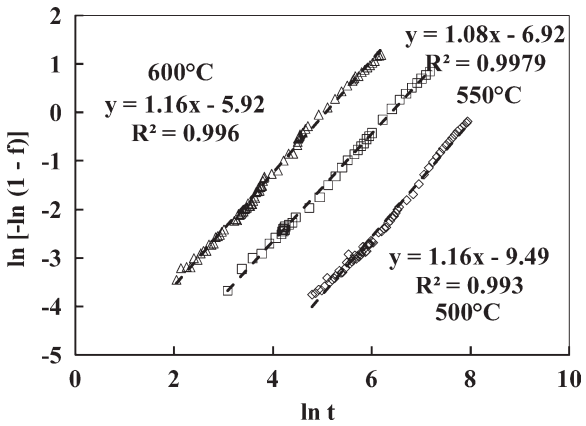

Figure 10. Avrami model plots for the isothermal annealing at different temperatures.

Values less than $f = 0.02$ were not used because of the difficulty in determining peak area.

Table 3. Estimated Kinetic Parameters for Pd-Cu Alloy Formation from a Bilayer

Temperature (°C)	k (1/min)	n	t_{99} (h)*
500	2.73×10^{-4}	1.16	225
550	1.62×10^{-3}	1.08	42
600	6.22×10^{-3}	1.16	10

*t_{99} refers to the amount of time required for 99% of the Pd-rich fcc alloy to form.

a one-dimensional, diffusion-controlled process and indicating a zero nucleation rate.[29] Table 3 shows that the Avrami exponents did not differ in the temperature range tested, indicating that the nucleation process was athermal. Of the works cited, the $CuGaSe_2$ formation had an athermal nucleation process,[14] while the Pd/Ag alloy[16] and $CuInSe_2$ formations[15] had Avrami exponents, which increased with temperature indicating that higher temperatures had overcome the nucleation barrier.

Ayturk et al.[16] attributed the temperature dependence of the Avrami exponents to the complete solid-phase miscibility of the Pd-Ag system where only compositional changes occurred. In the case of the Pd/Cu system, the bcc phase is a miscibility gap in the fcc phase (see Figure 1), and structural changes occurred in addition to compositional changes. Therefore, it should not be surprising that the nucleation process of the Pd/Cu system was different from that of the Pd/Ag system even though the systems are similar.

The rate constants shown in Table 3 indicated the length of time needed for the annealing process and the dependence of the annealing process on temperature. From the estimated parameters of the Avrami equation, the amount of time needed for 99% of the Pd-rich fcc alloy to form was calculated and listed in Table 3. Although a lengthy annealing time was required at 500°C, a relatively short annealing time was required at 600°C. It should be noted that these annealing times would only be sufficient to form a Pd/Cu layer with an fcc alloy on the surface and not a homogeneous layer, which would require higher temperatures or longer annealing times.

Figure 11 shows the fit of the experimental data to the Avrami model that has shown to be capable of describing the annealing of the Pd/Cu layer from the original bilayers. The model predicted the process quite well for the temperature range tested in this work.

Equation 4 shows the Arrhenius temperature dependence of the Avrami rate constant, and Figure 12 shows the regression used to estimate the activation energy, yielding a value of 175 kJ/mol, which corresponded with the range of the activation energies for the interdiffusion of Pd/Cu alloys, which ranged from 165 kJ/mol for a 10 wt % Cu alloy to 224 kJ/mol for a 80 wt % Cu alloy[31,32] rather than the activation energy for the fcc–bcc Bain transformation of 40 kJ/mol.[13] It would appear that the activation energy calculated from the Avrami rate constants corresponded to that of the diffusion of a low Cu content Pd/Cu alloy. However, the temperature range for the studies mentioned previously[31,32] was 800–1050°C.

$$k = A \exp\left[-\frac{E_a}{RT}\right]. \tag{4}$$

At low temperatures, diffusion occurs between the grain boundaries of metal, whereas at high temperatures diffusion occurs within the lattice of the grains. Lattice or bulk diffusion requires more thermal energy than grain boundary diffusion, and the activation energy for the bulk diffusion is higher than that of the grain boundary diffusion.[22] The transition temperature between the grain boundary and the bulk diffusion for Pd/Cu alloys was found by Bitler et al.[23] who studied the interdiffusion kinetics of wrought Pd/Cu diffusion couples and electroplated Pd on Cu in the temperature range of 550–900°C. For the wrought diffusion couples, at high temperatures, the activation energies varied between 203 and 273 kJ/mol for Cu compositions of 13–71 wt %, whereas at lower temperatures, activation energies varied between 90.2 and 123 kJ/mol for the same Cu compositions. The transition temperatures for grain boundary to bulk diffusion were found by extrapolating the linear regressions of the two diffusion regimes and varied between 745 and 772°C, depending on the alloy composition.

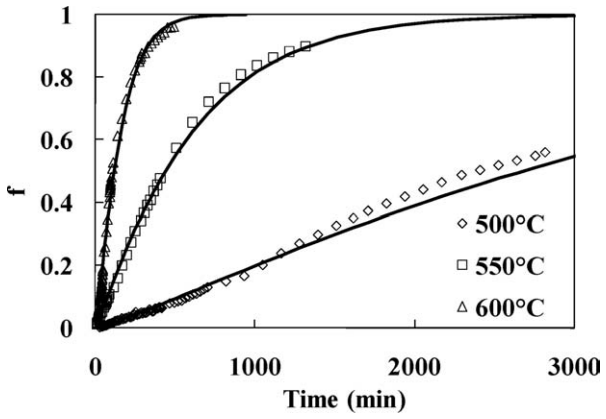

Figure 11. Weight fraction of the Pd-rich fcc phase as a function of time.

The solid lines correspond to the Avrami model.

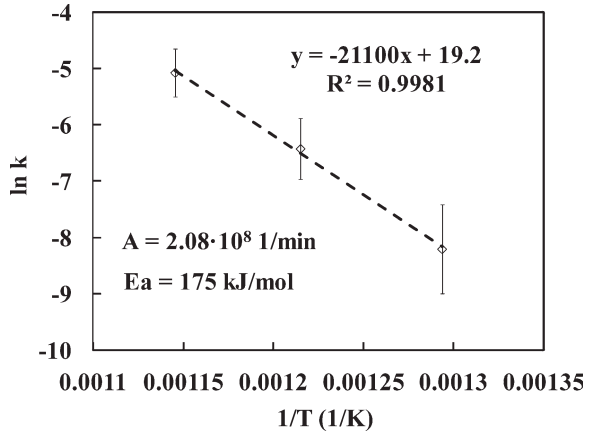

Figure 12. Arrhenius plot for the rate constants and the resultant activation energy based on the Avrami model.

Contrary to a single weld interface such as with wrought diffusion couples, the presence of many small grains in plated diffusion couples can significantly increase the overall area for diffusion. Whereas with the wrought couples, the area for diffusion would be equal to the area of the weld; with the plated Pd/Cu, the area would not only include the interface between the two metals but also the grain boundaries themselves. Decreasing the size of the grains would result in a higher area for diffusion. The diffusing atoms enter the grain boundaries and penetrate much more deeply into the opposing layer than with the wrought couple and enter the lattice of the grains from the grain boundaries. As a result, plated diffusion couples would have grain boundary diffusion even at higher temperatures.

Similarly, Bitler et al.[23] found activation energies for plated Pd/Cu couples, which were much lower than those of the bulk diffusion and varied less over the Cu concentration range tested. They found activation energies of 106–121 kJ/mol for compositions between 13 and 71 wt % Cu for the entire temperature range from 550 to 900°C. The grain size of the plated deposits was very small (10–20 nm), which allowed for grain boundary diffusion to occur at a much higher temperature than with the wrought Pd/Cu. No transition temperature was observed, showing that the grain size of the metal from the fabrication method of the diffusion couples affected the mechanism of the diffusion.

In addition, the diffusivities measured for the plated Pd/Cu were an order of magnitude higher than the diffusivities measured for the wrought Pd/Cu. Higher diffusivities are usually accompanied by lower activation energies, as was the case with the plated Pd/Cu. Similarly, Chow et al.[33] investigated the diffusion of electrodeposited Pd on Cu substrates between the temperatures of 300 and 700°C and also found that the activation energies did not differ greatly with Cu composition, varying between 102 and 116 kJ/mol for compositions ranging between 20 and 80 wt % Cu. The activation energies were also significantly lower than activation energies for wrought Pd/Cu and for the bulk diffusion regime.

Al-Kassab et al.[34] measured diffusion coefficients for a composition of 37 wt % Cu at 300 and 350°C and extrapolated their results to those of previous studies performed at high temperatures[31,32] to show that the activation energy was similar. Philofsky and Hilliard[35] found activation energies of 204 and 277 kJ/mol for Cu compositions of 20 and 5 wt %, respectively, between the temperatures of 355 and 440°C.

The samples by Al-Kassab et al.[34] consisted of sputter deposited layers of Pd and Cu of a total thickness of 20 nm. The reason that the low temperature data[34] yielded an activation energy corresponding to bulk diffusion at low temperatures was due to the very few grain boundaries present in the sample because of the method of deposition, thus producing bulk diffusion at a low temperature. The submicron films of Philofsky and Hilliard[35] contained short wavelength composition modulations produced by evaporation, upon which the interdiffusion coefficients were dependent. They theorized that extrapolating the wavelengths to infinity yielded true bulk diffusion coefficients at low temperatures.

The studies of Bitler et al.,[23] Chow et al.,[33] Al-Kassab et al.,[34] and Philofsky and Hilliard[35] showed that the fabrication method of Pd/Cu diffusion couples not only influenced

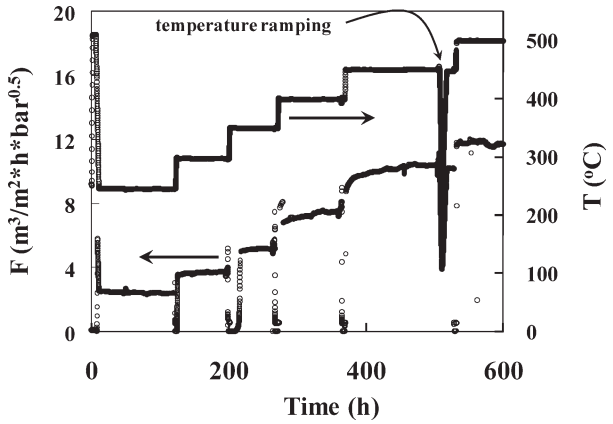

Figure 13. Permeance of the Pd/Cu membrane as a function of time.

the value of the interdiffusion coefficients measured but also the mechanism of the diffusion, as seen by measuring the activation energy. Although Bitler et al.[23] were the only group that measured the actual grain size, they together with Chow et al.[33] and Al-Kassab et al.[34] all attributed the deviation from the expected diffusion regime to the grain size.

The Avrami activation energy calculated in this work was significantly higher than the activation energies reported for electrodeposited Pd/Cu samples, which were slightly larger than the activation energies of grain boundary diffusion. The difference could be due to the grain size. The measured grain sizes of electrolessly deposited Pd were previously estimated by XRD and TEM (transmission electron microscopy) to be roughly 50 nm,[36] which were larger than the grain sizes measured by Bitler et al.,[23] most likely due to the method of deposition, the former using electroless plating and the latter using electroplating.

In addition, the grain growth of the Pd was found to be significantly larger in a H_2 atmosphere than in an inert He atmosphere. After 48 h in He at 500°C, Pd grains had grown to a size of 70–100 nm, whereas after 48 h in H_2, the grains had grown to 100–200 nm (as measured by TEM).[36] In contrast to the hydrogen atmosphere used in this work, the diffusion experiments mentioned previously[23,33] were performed in evacuated quartz tubes.

The activation energies measured for the electrodeposited couples were higher than those of grain boundary diffusion for wrought diffusion couples, which had grain sizes several orders of magnitude larger on the order of $\sim$100 μm. As it has been shown that grain size did affect the diffusion mechanism,[23,33,34] it is possible that even though the temperatures tested in this work were below the transition temperature for the grain boundary/bulk diffusion mechanism, the larger grain size in this work than those mentioned previously[23] caused by the different deposition conditions and the subsequent annealing in H_2 increased the activation energy of diffusion to a value closer to that of bulk diffusion than grain boundary diffusion.

Furthermore, the H_2 atmosphere used in this work would enhance the diffusion process by increasing the lattice constant of the alloy, as hydrogen does with pure Pd, although to a lesser extent as H_2 is less soluble in Pd/Cu alloys.[37] The H_2 enhanced diffusion could also enable bulk diffusion to

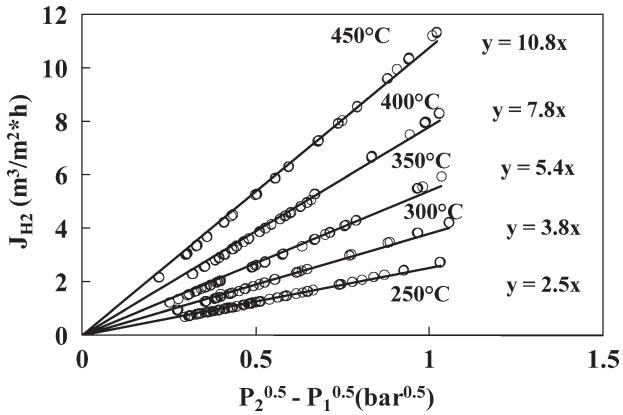

Figure 14. Sieverts' law regressions for the Pd/Cu membrane.

The R^2 values from the linear regressions were close to 1.

take place at a lower temperature than without the presence of H_2. Thus, the rate-determining process for the solid-state transformation was the bulk diffusion of Cu into Pd. Ayturk et al.[16] had also observed an activation energy, which corresponded to bulk diffusion for the Pd/Ag bilayers annealed in H_2, rather than grain boundary diffusion; however, no discussion was given by Ayturk et al.[16] with regards to the two diffusion regimes.

Membrane permeation

The total bilayer thickness on the oxidized Inconel support was 12.5 μm Pd and 1.5 μm Cu resulting in a total composition of 8 wt % Cu. Figure 13 shows the characterization of the Pd/Cu membrane between the temperatures of 250 and 450°C. Before characterization, the membrane was preannealed for 5 h at 500°C in H_2 to cause the Pd/Cu layers to alloy. Although the H_2 permeance stabilized fairly quickly (<24 h) upon reaching the testing temperatures at 250, 300, and 350°C, the permeance required ~100 and 150 h to stabilize at 400 and 450°C, respectively, indicating that the Pd/Cu layer was continuing to anneal. The He leak of the membrane was undetectable for this temperature range.

After the permeance stabilized at each temperature, the permeance (F) was calculated in accordance with Sieverts' law, shown in Figure 14 and Eq. 5. The linear dependence of the H_2 flux (J_{H2}) on the difference of the square root of the transmembrane pressure (P) indicated that the H_2 permeation was one dimensional and limited by the diffusion of H_2 through the Pd/Cu layer.

$$J_{H_2} = F \cdot \left(P_2^{0.5} - P_1^{0.5}\right). \quad (5)$$

The permeance calculated from the Sieverts' law regression at various temperatures was plotted in Arrhenius fashion to calculate the activation energy, shown in Figure 15. The activation energy from the characterization between 250 and 450°C was 21.0 kJ/mol. After the permeance stabilized at 450°C, the activation energy was calculated again to determine how the high temperature had affected the H_2 permeance. The temperature of the membrane was ramped at a rate of 0.5°C/min, while the H_2 permeance was simultaneously measured at a pressure difference of $\Delta P = 1$ bar ($P_1 = 1$ bar, shown in Figure 13 at 525 h). The method of calculating the activation energy by ramping the temperature was described in detail previously.[11] As seen in Figure 15, the permeance had increased at lower temperatures, resulting in a lower activation energy of 14.6 kJ/mol, showing that the structure of the membrane had changed at 450°C.

According to Figure 7, the preannealing at 500°C would have resulted in ~30% of the bcc phase forming within the XRD penetration depth of the layer if not more, as the heating/cooling rate of the membrane during the preannealing was 1°C/min, which was much slower than the heating/cooling rate of the furnace used with the HT-XRD analysis. Although the characterization of the membrane between the temperatures of 250 and 350°C did not provide enough thermal energy to cause further diffusion of the Cu into the Pd layer, heating at 400 and 450°C did cause additional annealing of the layer, increasing the amount of the bcc phase as the bcc phase had not yet reached the maximum seen in Figure 7. As a result, the permeance increased because of the higher permeability of the bcc phase.[8]

The high activation energy of 21.0 kJ/mol before the structure change was due to the steep gradient of Cu within the Pd/Cu layer increasing the mass transfer resistance of the layer to H_2 transport. The increased Cu content in a Pd/Cu fcc alloy decreased the lattice constant and would affect both the diffusion and the solubility of hydrogen atoms in the lattice.[6] The increase in the permeance seen with the formation of more of the bcc phase was accompanied by a decrease in mass transfer resistance within the Pd/Cu layer and the activation energy decreased.

Figure 16 shows the continued testing of the Pd/Cu membrane at 500°C. The permeance decreased within the first 200 h by 26% (from 12 m^3/m^2 h $bar^{0.5}$ to 8.9 m^3/m^2 h $bar^{0.5}$) and then remained stable for the duration of the high temperature testing. The ideal H_2/He separation factor decreased from 3980 to 350 during the long-term testing at 500°C because of the grain growth.[38] According to the predictions of the Avrami model, the time required for the bcc phase to disappear (t_{99} in Table 3) at 500°C was 225 h, which was close to the time duration of the decrease in permeance. In addition, the activation energy of permeation

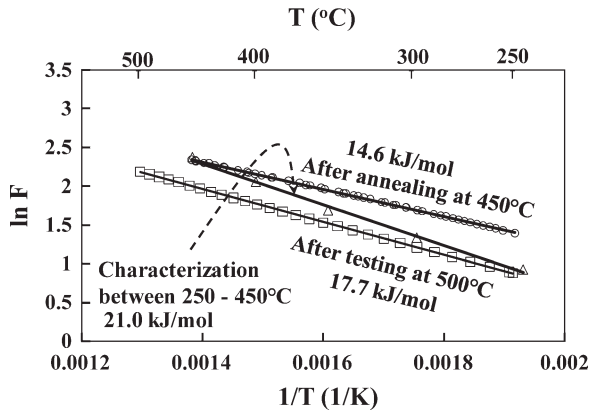

Figure 15. Activation energy of the Pd/Cu membrane before and after different stages of annealing.

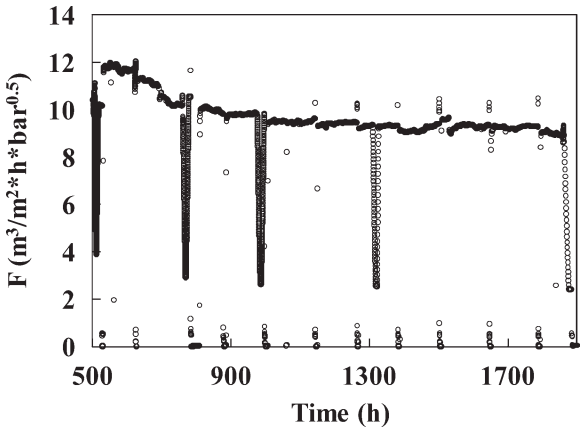

Figure 16. Permeance of the Pd/Cu membrane at 500°C.

measured after 1300 h at 500°C slightly increased to 17.7 kJ/mol. The transformation of the bcc phase to the fcc phase would be accompanied by a decrease in the H_2 permeance and increase in activation energy of permeation.

The decrease in the permeance seen in Figure 16 was again explained by the findings of the Avrami model, showing that the Avrami model could be used not only to describe the annealing mechanism of the Pd/Cu bilayers but also to describe the increase in permeance seen at 450°C and the accompanying decrease in the activation energy and the decrease in the permeance at 500°C and the accompanying increase in activation energy caused by the phase change.

Discussion

An important note with the coupon experiments was that disappearance of the bcc phase never occurred even after the lengthy annealing time at 500°C. Because of the one-dimensional direction of the Cu diffusion, the remaining bcc phase would be on the surface of the sample. The total concentration of the Pd/Cu bilayers was roughly 15 wt % (see Table 2), which would place the total composition of the layer in the Pd-rich fcc phase portion of the Pd-Cu phase diagram (see Figure 1). However, at the end of the annealing at 500°C, 40 wt % of the bcc phase was still present, which contradicted the results of the EDX analysis of both the surfaces and cross sections that showed that Cu concentrations were no higher than 20 wt %. It was likely that the bcc phase was present in certain areas of the porous Pd/Cu alloy seen in Figures 5b–d, but that the roughness of the porous alloy made pinpointing where the bcc phase was more difficult because of the EDX resolution.

A H_2 atmosphere did cause a slight shift of the Pd/Cu miscibility gap to greater Pd compositions by 3 at %.[39] Also, it is possible that the EDX was not as accurate in determining Cu composition as a composition of 34 wt % (taking into account the shift caused by the H_2 atmosphere) was needed at 500°C in order for the bcc phase to still be present. The coupons annealed at different temperatures all completed the annealing with different ratios of the fcc/bcc phases. However, there was little difference between them in the cross-sectional line scans and the surface area scans, showing that EDX was not able to differentiate between them.

As for the fabrication of Pd/Cu membranes for catalytic membrane reactors, when mass produced on an industrial scale, many steps can be shortened or removed completely. With 24-h automated production, the total fabrication time of a batch of dense Pd membranes could be cut down to several days, reducing the production cost considerably. With regards to adding Cu for sulfur resistance, the preferred annealing time would depend on the required level of hydrogen purity in the permeate stream. Although annealing at 600°C would be less expensive and result in a quickly formed fcc alloy, it is likely that a membrane annealed in this manner would form leaks due to grain coarsening, likewise with annealing at 550°C.[38] If the hydrogen purity needed is less than 99.5%, then the high temperature annealing would be less time consuming, more cost effective, and therefore preferable. Higher purity hydrogen in the permeate stream would require a lower annealing temperature even though the membrane preparation would take longer to complete and the fabrication process would be more expensive.

Conclusions

By implementing HT-XRD and calculating the weight fractions of the phases, this work has successfully applied the Avrami model to investigate the annealing process of Pd/Cu bilayers to form the sulfur-resistant fcc Pd/Cu alloy. The Avrami exponent of 1.1 indicated that the nucleation and growth of the fcc phase were one dimensional in nature, and that the nucleation itself was athermal because of a lack of dependence of the Avrami exponent on temperature. The activation energy calculated from the Avrami rate constants was 175 kJ/mol and indicated that the rate-limiting process of the solid-state transformation was the bulk diffusion of Cu into Pd. The experimental data fit well to the Avrami model, and the model showed 225 h would be needed to completely form the fcc phase from Pd/Cu bilayers at 500°C. The higher temperatures would be detrimental to the selectivity of a membrane due to grain coarsening and pinhole formation.

Finally, the Pd/Cu membrane was characterized between the temperatures of 250 and 500°C, and changes occurred both in permeance and activation energy following phase transformations at higher temperatures. The Avrami model explained both the change in the permeation and activation energy over time as the amount of the more permeable bcc phase increased and then decreased in favor of the less permeable fcc phase.

Acknowledgments

The authors express their gratitude to the University Coal Research Program, U.S. Department of Energy for the financial support under Award No. DE-FG26-04NT42194. This research at the Oak Ridge National Laboratory's High Temperature Materials Laboratory was sponsored by the U.S. Department of Energy, Office of Energy Efficiency and Renewable Energy, Vehicle Technologies Program.

Notation

A = Arrhenius constant, 1/min
E_a = activation energy, J/mol
F = hydrogen permeance, m^3/m^2 $bar^{0.5}$ h
f = fraction of new phase, no unit

G_x = diffracted intensity, no unit
J_{H_2} = hydrogen flux, m^3/m^2 h
k = Avrami rate constant, 1/min
n = Avrami exponent, no unit
P = pressure, bar
R = gas constant, J/mol K
T = temperature, K
t = time, min
x = distance from surface, cm
μ = linear absorption coefficient, 1/cm

Literature Cited

1. Bredesen R, Jordal K, Bolland O. High-temperature membranes in power generation with CO_2 capture. *Chem Eng Process*. 2004;43: 1129–1158.
2. McKinley DL. Metal alloy for hydrogen separation and purification. US Pat. 3,350,845, 1967.
3. Mundschau MV, Xie X, Evenson CR, Sammells AF. Dense inorganic membranes for production of hydrogen from methane and coal with carbon dioxide sequestration. *Catal Today*. 2006;118:12–23.
4. Kajiwara M, Uemiya S, Kojima T. Stability and hydrogen permeation behavior of supported platinum membranes in presence of hydrogen sulfide. *Int J Hydrogen Energy*. 1999;24:839–844.
5. Kulprathipanja A, Alptekin GO, Falconer JL, Way JD. Pd and Pd-Cu membranes: inhibition of H_2 permeation by H_2S. *J Membr Sci*. 2005;254:49–62.
6. Subramanian PR, Laughlin DE. Cu-Pd (copper-palladium). *J Phase Equilib*. 1991;12:231–243.
7. Morreale BD, Ciocco MV, Howard BH, Killmeyer RP, Cugini AV, Enick RM. Effect of hydrogen-sulfide on the hydrogen permeance of palladium-copper alloys at elevated temperatures. *J Membr Sci*. 2004;241:219–224.
8. McKinley DL. Method for hydrogen separation and purification. US Pat. 3,247,648, 1966.
9. Knapton AG. Palladium alloys for hydrogen diffusion membranes. *Platinum Met Rev*. 1977;21:44–50.
10. Gryaznov V. Metal-containing membranes for the production of ultrapure hydrogen and the recovery of hydrogen isotopes. *Sep Purif Methods*. 2000;29:171–187.
11. Pomerantz N, Ma YH. Effect of H_2S on the performance and long-term stability of Pd/Cu membranes. *Ind Eng Chem Res*. 2009;48: 4030–4039.
12. Ma YH, Akis BC, Ayturk ME, Guazzone F, Engwall EE, Mardilovich IP. Characterization of intermetallic diffusion barrier and alloy formation for Pd/Cu and Pd/Ag porous stainless steel composite membranes. *Ind Eng Chem Res*. 2004;43:2936–2945.
13. Guazzone F. Engineering of substrate surface for the synthesis of ultra-thin composite palladium and palladium-copper membranes for hydrogen separation. PhD Dissertation. Worcester, MA: Worcester Polytechnic Institute, 2006.
14. Kim WK, Payzant EA, Kim S, Speakman SA, Crisalle OD, Anderson TJ. Reaction kinetics of $CuGaSe_2$ formation from a GaSe/CuSe bilayer precursor film. *J Cryst Growth*. 2008;310:2987–2994.
15. Kim S, Kim WK, Kaczynski RM, Acher RD, Yoon S, Anderson TJ, Crisalle OD, Payzant EA, Li SS. Reaction kinetics of $CuInSe_2$ thin films grown from bilayer InSe/CuSe precursors. *J Vac Sci Technol A*. 2005;23:310–315.
16. Ayturk ME, Payzant EA, Speakman SA, Ma YH. Isothermal nucleation and growth kinetics of Pd/Ag alloy phase via in situ time-resolved high-temperature X-ray diffraction (HTXRD) analysis. *J Membr Sci*. 2008;316:97–111.
17. Ma YH, Mardilovich PP, She Y. Hydrogen gas-extraction module and method of fabrication. US Pat. 6,152,987, 2000.
18. Mardilovich PP, She Y, Ma YH, Rei M. Defect-free palladium membranes on porous stainless-steel support. *AIChE J*. 1998;44: 310–322.
19. Ma YH, Mardilovich IP, Engwall EE. Thin composite palladium and palladium/alloy membranes for hydrogen separation. *Ann N Y Acad Sci*. 2003;984:346–360.
20. Cullity BD, Stock SR. *Elements of X-Ray Diffraction*. New Jersey: Prentice Hall, 2001.
21. Samsonov GV. *The Oxide Handbook*. New York: IFI/Plenum, 1973.
22. Porter DA, Easterling KE. *Phase Transformation in Metals and Alloys*. London: Chapman and Hall, 1981.
23. Bitler WR, Pickering HW, Kaja S. Interdiffusion kinetics of copper with palladium. *Plat Surf Finish*. 1985;72:60–63.
24. Yuan L, Goldbach A, Xu H. Permeation hysteresis in PdCu membranes. *J Phys Chem B*. 2008;112:12692–12695.
25. Butrymowicz DB, Manning JR, Read ME. Diffusion in copper and copper alloys. IV. Diffusion in systems involving elements of Group VIII. *J Phys Chem Ref Data*. 1976;5:103–200.
26. Avrami M. Kinetics of phase change. I. General theory. *J Chem Phys*. 1939;7:1103–1112.
27. Avrami M. Kinetics of phase change. II. Transformation-time relations for random distribution of nuclei. *J Chem Phys*. 1940;8:212–224.
28. Avrami M. Granulation, phase change and microstructure. Kinetics of phase change. III. *J Chem Phys*. 1941;9:177–184.
29. Hulbert SF. Models for solid-state reactions in powdered compacts. *J Br Ceram Soc*. 1969;6:11–20.
30. Christian JW. *Theory of Transformations in Metals and Alloys. I. Thermodynamics and General Kinetic Theory*. New York: Pergamon, 1978.
31. Borovskii IB, Marchukova ID, Ugaste YE. Interdiffusion in binary systems forming a continuous series of solid solution by using a local x-ray spectral analysis. The iron-palladium, cobalt-palladium, nickel-palladium, and copper-palladium systems. *Fiz Met Metalloved*. 1966;22:849–858.
32. Badia M. Interdiffusion of Fe and the transition metals. PhD Dissertation. Nancy, France: University of Nancy, 1969.
33. Chow KM, Ng WY, Yeung LK. Barrier properties of Ni, Pd and Pd-Fe for Cu diffusion. *Surf Coat Technol*. 1998;105:56–64.
34. Al-Kassab T, Macht M, Wollenberger H. FIM/AP analysis of Cu-Pd multilayers. *Appl Surf Sci*. 1995;87/88:329–336.
35. Philofsky EM, Hilliard JE. Effect of coherency strains on diffusion in copper-palladium alloys. *J Appl Phys*. 1969;40:2198–2205.
36. Saini A. An investigation of the cause of leak formation in palladium composite membranes. MS Thesis. Worcester, MA: Worcester Polytechnic Institute, 2006.
37. Lewis FA. *The Palladium-Hydrogen System*. London: Academic Press, 1967.
38. Guazzone F, Ma YH. Leak growth mechanism in composite Pd membranes prepared by the electroless deposition method. *AIChE J*. 2008;54:487–494.
39. Piper J. Diffusion of hydrogen in copper-palladium alloys. *J Appl Phys*. 1966;37:715–721.

Manuscript received Sept. 15, 2009, and revision received Feb. 3, 2010.